High-displacement flexible Shape Memory Alloy actuator for soft wearable robots

Article *in* Robotics and Autonomous Systems · January 2014

DOI: 10.1016/j.robot.2014.09.026

CITATIONS
23

READS
993

5 authors, including:

Alvaro Villoslada
Marsi Bionics
11 PUBLICATIONS **50** CITATIONS
SEE PROFILE

Antonio Flores-Caballero
University Carlos III de Madrid
20 PUBLICATIONS **72** CITATIONS
SEE PROFILE

Dorin Copaci
University Carlos III de Madrid
28 PUBLICATIONS **73** CITATIONS
SEE PROFILE

Dolores Blanco
University Carlos III de Madrid
85 PUBLICATIONS **682** CITATIONS
SEE PROFILE

High-displacement flexible Shape Memory Alloy actuator for soft wearable robots

A. Villoslada, A. Flores, D. Copaci, D. Blanco, L. Moreno

Universidad Carlos III de Madrid, Avda. Universidad 30, 28911-Leganés, Spain

Abstract

This paper describes a flexible Shape Memory Alloy (SMA) actuator designed to increase the limited displacement that these alloys can induce. The SMA actuator has been designed so that it can be bent up to about 180 degrees, providing more freedom of movements and a better integration in wearable robots, specially in soft wearable robots, than standard rigid solutions. Although the actuator length is relatively short, this original design allows a great linear displacement, because it can have one or more loops of the same SMA wire inside the actuator. This implies that the length of the SMA wire is at least two times greater than the length of the actuator. The adopted strategy for both position and speed control that overcomes the hysteresis and prevents overheating the actuator is also described. The control algorithm has been implemented in a rapid control prototyping (RCP) system based on a low cost hardware platform. Finally, the application of this novel actuator in a wrist exoskeleton prototype is shown to demonstrate the feasibility of using the flexible SMA actuator in a real soft wearable robot.

Keywords:
SMA actuator, Flexible actuator, Rapid Control Prototyping, Hammerstein-Wiener model, Position and velocity control

1. Introduction

Thanks to the progressive miniaturization of technology (electronic components, energy sources...) and the advances in new materials, wearable robotics is becoming an emerging field within robotics research; the number of publications, prototypes and even commercial devices has increased significantly over the last years. Rehabilitation is one of the areas where wearable robotics has an important niche application. Rehabilitation often involves the displacement of the patient to a health center where a specialist will perform a series of exercises designed to restore or improve the mobility of the member to rehabilitate. Sometimes, precisely due to the physical problem to be rehabilitated, the patient must use an ambulance to travel to the health center, increasing the cost of the treatment. In addition to this, rehabilitation exercises are tedious and repetitive for the physiotherapist, and in some cases more than one specialist is needed to perform them. For these reasons, the use of a portable wearable robot to perform rehabilitation exercises is very advantageous: the patient can use it at home without the need to move to a health center; the robot can operate autonomously with preprogrammed exercises or the physiotherapist can operate the robot remotely; thanks to the sensors in the device, precise measurements of the effectiveness of the treatment can be obtained; as the robot does not get tired, the exercises can be repeated as many times as the patient wishes. Not all wearable robots feature the above advantages, some suffer from the same disadvantages than classical rehabilitation methods regarding the need to travel to a health center. These are rigid exoskeletons that, due to the weight of their actuators and mechanical structure, are attached to a structure fixed to the floor. Soft exoskeletons, a new trend in the field of wearable robots, aim to solve these issues and achieve the design of fully portable devices. In a soft exoskeleton the rigid structure that supports the actuators is the skeletal structure of the wearer. A soft exoskeleton is lighter, less bulky, more comfortable and more adaptable to the body of the user than its rigid counterpart. The joints are attached to the actuators by means of cables, placing the actuators outside the limbs (usually on the user's back), with the advantages of reduced weight and inertia on the limbs that this entails.

Wearable robots have to be as comfortable, portable and lightweight as possible, specially rehabilitation robots because they should interfere as little as possible in the exercises performed by the patient. However, the development of fully portable and lightweight wearable robots is limited by the actuation systems needed to drive their joints. While technological development has led to a significant miniaturization of sensors and control systems, the actuators for robotic devices have not undergone similar development. Actuators transform energy, mainly between the electrical and the mechanical domains, with the aim of imposing a mechanical state on a system they drive. This process should not be influenced by perturbations, making power delivery one of the most important parameters of the actuator, usually at the expense of a larger size [1]. However, there are some actuators that, despite their small size, can deliver a considerable power. SMA actuators are within this type of actuators.

A Shape Memory Alloy (SMA) is a metallic alloy that can recover its original "memorized" shape after being deformed when heated above its transformation temperature, due to a transition between a martensite phase (low temperature) and an austenite phase (high temperature). The most common of these alloys used for actuation is Nickel-Titanium, or Nitinol. The deformation-recovery cycle of Nitinol can be repeated millions of times, provided that the applied deformations are in the recovery range of the alloy, thanks to one of its features: superelasticity. A SMA actuator uses a SMA element as the transducing material of the actuator: the SMA transducer converts thermal energy into mechanical work. If the SMA element is heated by means of the Joule effect, with a simple circuit that applies an electric current to the SMA actuator, two transduction processes take place. First, electric energy is transformed into thermal energy thanks to the Joule effect. This thermal energy triggers the shape recovery process of the SMA element and the resulting recovery energy is transformed into mechanical work. SMAs have several advantages when used as actuators for robotic applications, especially in wearable robotics. They are small and lightweight, which allows for a reduction in size, weight and complexity of the robotic devices. The force-to-weight ratio is very high: a $510\mu m$ diameter Flexinol® wire can exert a force in tensile deformation of about $35N$ [2]. When using SMA wires in tensile deformation, the actuation resulting from the deformation-recovery cycle is similar to the behaviour of a human muscle. Finally, their operation is quiet, a very desirable feature for wearable robots.

Among the general limiting factors of SMA actuators (nonlinear operation, low actuation bandwidth, low efficiency), one of the features of SMA wires that work in a linear way (contracting and stretching) is the low strain they can achieve, typically 2% to 5% of their length. If a long straight wire is used to obtain a great displacement, the actuator is no longer compact, which is particularly undesirable in some applications like wearable assistive devices, wearable rehabilitation robots or robotic prosthesis. SMA springs can also be used to achieve a great linear displacement, but the force exerted by the spring is less than that exerted by a straight wire.

The purpose of this paper is to describe the design of a SMA actuator with the aim of solving one of the shortcomings that SMA exhibit when used as actuators for robotic devices, namely: their low strain-to-lenght ratio. The actuator described here is designed to achieve mechanical motion amplification with a more compact design than a long straight wire and capable to exert a force greater than a spring. Also, the implemented control algorithm for the actuator overcomes the problem of the nonlinearity of the SMA and enhances its actuation bandwidth and service life by preventing overheating.

2. Actuator design

To design a high-displacement compact SMA actuator using a long wire, the common approach is to wrap the wire around a pulley array. The disadvantage of this solution is that if the length of the wire increases, more pulleys are needed to keep the actuator compact, increasing the complexity and weight of the actuator and its frictional losses. An actuator based on this principle, intended to actuate a prosthetic hand, is described in [3]. This actuator consists of a single SMA wire folded to form two parallel branches so that the force that the wire exerts is doubled. The folded wire is wrapped around two miniature pulleys to reduce the total length of the actuator. With this arrangement, the designed actuator has a length of $147mm$ and can contract more than $15mm$, representing over a 10% of the total actuator length. In [4], another pulley-based compact SMA actuator, designed to actuate an ankle rehabilitation device, is presented. The actuator is a $83cm$ SMA wire routed back-and-forth between two arrays of ten pulleys inside an

insulated cartridge. The actuator can achieve a linear stroke of 2.5cm.

In the particular case of wearable robots, usually great angular or linear displacements are required to mobilize the limbs. For example, to flex the wrist 90 degrees, the actuator should produce a linear displacement of about 5cm. If the SMA wire is contracted a 3% of its length, in order to increase its service life, a 1.67m wire would be needed. A very compact actuator capable of obtaining such a large output displacement would require a lot of pulleys, with the problems related with frictional losses and total weight of the actuator this entails. On the other hand, placing such a long wire in a straight configuration is infeasible in almost any robot, and specially in a wearable device. But, what if the SMA wire could be bent and still able to transmit force and movement? In this way, the two ends of the actuator could be fixed on different parts of a soft wearable robot, and the actuator itself could be bent to adapt it to the shape of the structure where it would be installed; in the case of an actuator for a wearable robot, the user's body. This is the solution presented in this paper and the way to achieve this has been to use a Bowden cable transmission system that serves as a guide for the SMA wire and allows the actuator to bend.

A Bowden cable is a mechanical transmission system consisting of a flexible inner cable and a flexible outer sheath. Normally, in a Bowden cable actuation system, the actuator is mechanically connected to the the joint to be actuated through a cable, and located away from the joint. The force is applied to the joint by mechanical displacement between the cable and the outer sheath. The actuator presented in this paper is based on this principle, with the difference that the element that exerts force on the joint, the SMA wire, is not located away from the joint, but rather is guided inside the flexible Bowden cable sheath.

Besides using a Bowden cable system to have a long SMA wire capable of producing a large displacement and that can be adapted to the shape of the device it actuates, the actuator has been designed so that its length is less than the total length of the wire. To shorten the actuator, the design is based on the method of wrapping a long straight wire around a number of pulleys. Only two pulleys are used to reduce the complexity, weight and frictional losses of the actuator. Two rigid pieces to house the pulleys are located at both ends of the Bowden cable sheath. This two rigid ends of the actuator can be fixed on different parts of a soft wearable robot and the Bowden cable sheath acts as a flexible interface that connects them.

A CAD model of the actuator is shown in Figure 1. The actuator is composed of two fundamental parts: the terminal units and the Bowden cable sheath that connects them. The terminal units are two small aluminium boxes of 22x12x7mm with a hollow part of 10x10mm, where an aluminium pulley with a diameter of 7mm is housed. The two ends of the boxes have a threaded hole. One of the ends is where the fastening piece of the Bowden cable sheath is screwed. The piece which fixes the terminal unit to the device, securing the actuator, is screwed into the other threaded hole.

The Bowden cable sheath is made of nylon. The two ends of the sheath are pressed into two cylindrical pieces of aluminium, shown in the detail of Figure 1. This pieces are threaded to screw them into the holes of the terminal units, connecting the Bowden cable sheath to both units. The interior of these fastening pieces is traversed by a cylindrical conduit through which the SMA wire passes toward the pulleys. One end of the SMA wire is clamped to one of the fastening terminals of the Bowden cable sheath. The wire is passed through a hole perpendicular to the fastening piece and secured pressing it against the terminal unit of the actuator by means of a nut.

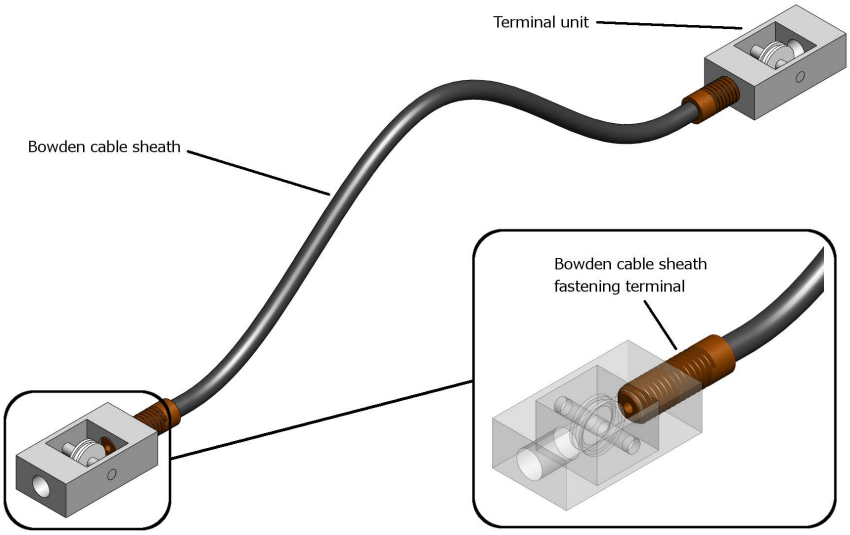

Figure 1: CAD model of the flexible SMA actuator

As stated above, the SMA wire is wrapped around the two pulleys housed in the terminal units of the actuator, so that there are three branches of the SMA wire inside the Bowden cable sheath. This means that the length of the SMA wire is three times the length of the actuator, thereby increasing the ratio between the displacement and the total length of the actuator. The arrangement of the SMA wire inside the actuator is shown in Figure 2. The wire is fixed to the left terminal unit (Figure 2 - B). and the movable end of the SMA wire passes through the right terminal unit (Figure 2 - C).

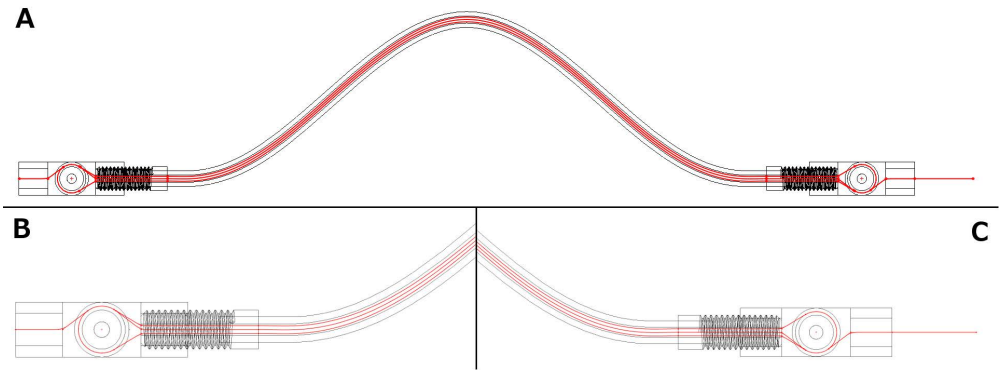

Figure 2: Layout of the SMA wire inside the actuator

The designed actuator is shown in Figure 3 together with a detailed view of one of the terminal units, with the SMA wire coming out of the Bowden cable sheath, wrapping around the pulley and going back into the sheath. In this set-up, one of the ends of the actuator is fixed to a wooden surface, while the movable end can be attached to a suspended mass whose weight provides a constant bias load that restores the length of the SMA wire during the cooling phase.

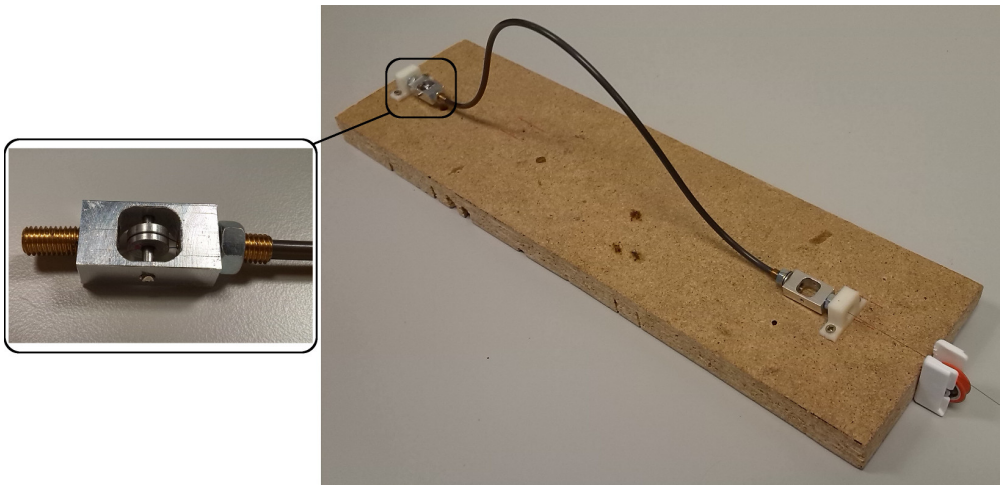

Figure 3: The designed flexible SMA actuator

2.1. Power electronics

In order to heat the SMA wire, which is necessary to activate its shape memory effect and thus contract it, a controlled electric current is passed through the wire. This electric current is provided by a high fidelity commutation circuitry, driving an extremely low on resistance (about $2m\Omega$) state of the art MOSFET transistor (STMicroelectronics® STP310N10F7) with a pulse width modulated (PWM) signal from the microcontroller [5]. The average value of the output current is directly dependant on the pulse width:

$$\bar{O} = D * O_{Max} + (1 - D) * O_{Min} \tag{1}$$

Equation 1 expresses the average value of the output for a PWM signal, where D is the Duty Cycle, O_{Min} is the minimun value of the output and O_{Max} is the maximum value of the output.

The power electronic hardware is optocoupled from the control unit, providing enhanced security for the user and for all connected equipment. Power is supplied by a simple AC/DC converter or by dry cell batteries.

3. Actuator control

3.1. Control electronics

Traditionally, the development of the embedded software, also called firmware, comprises many processes such as the selection and design of the embedded controller, programming the MCU (usually via hand-written languages), running and testing the program, as well as the verification of the required execution time and its performance. All these embedded controller design stages need to be started over each time an error or malfunction is detected, making the implementation of really large and complex firmwares a time and money consuming task [6].

In the development of the embedded firmware that provides total control, data acquisition and processing for the designed actuator, a methodology based on the usage of a Rapid Control Prototyping (RCP) software/hardware tools have been used. A RCP offers a great set of interesting features; all the previously mentioned stages for firmware development can be accomplished using the same unified hardware platform, making possible the conduction of as many tests and iterations as needed in less time than with traditional methods. Usually a RCP system provides a higher level of abstraction than other methods thanks to the usage of graphical programming languages. Due to the high level of abstraction, the complex nature of many input/output (I/O) analog and digital interfaces can be obviated, making the usage of a RCP system possible for a multidisciplinary audience [7, 8], allowing for an easy integration

of multiple analog, digital and communication interfaces at same time for a standalone controller.

The RCP system used to implement the control system for the actuator presented in this article is an in-house development of the RoboticsLab at the Carlos III of Madrid University (UC3M). The RCP is based on a System-On-Chip (SOC) embedded system, consisting of a state of the art 32-Bit MCU running at 168 - 180MHz with floating point support via hardware (STM32F407 and STM32F429 families from ST Microelectronics®), that provides plenty digital and analog interfaces requiring no external add-on hardware. This MCU is capable of fully autonomous function and can also be driven externally via digital interfaces like Universal Serial Bus (USB) or Controller Area Network (CAN Bus), or analogically via analog inputs. The SOC RCP based solution proves itself to be the most competitive prototyping solution for both cost and performance [7, 9, 10]. The computational power of the UC3M RoboticsLab RCP system is almost twice the required by more than 50% of industrial production-ready control devices, that commonly require a 16 - 32 bit MCU running at 10 - 99MHz with no floating point hardware support, and no more than 25% of the devices require clock speeds far beyond 100MHz [11, 12]. These features, and the small footprint size and minimal power consumption, make the described UC3M RCP system ideal for laboratory prototyping as well as for final hardware implementation.

The high level of abstraction for the development of embedded software for the RCP system is provided by the use o Matlab/Simulink® that provides a graphical programming language, ideal for the development of control systems. As can be seen in Figure 4, the Matlab/Simulink® programming environment uses simple appearance blocks that can be interpreted as configurable modular pieces of code implementing different features. Each block is completely tested and debugged during its implementation, ensuring that more complex systems based on these modules will work flawlessly. To use the proposed RCP system alongside Matlab/Simulink®, the installation of additional software is required. This additional software consists of two custom developed blocksets, requiring no additional commercial software like Embedder Coder® [7, 9] or xPC Target® [13]. The first blockset, provided by Aimagin Ltd. for free, works as base software and covers many I/O peripherals of the MCU. The second of the required blocksets works as an extension of the previous one. It has been entirely developed by the UC3M RoboticsLab and is the core of the proposed RCP system, providing high speed USB data exchange links with Matlab/Simulink® and advanced features like Real-Time multitasking support, complete I/O peripherals and some very specialized performance optimizations to the generated code.

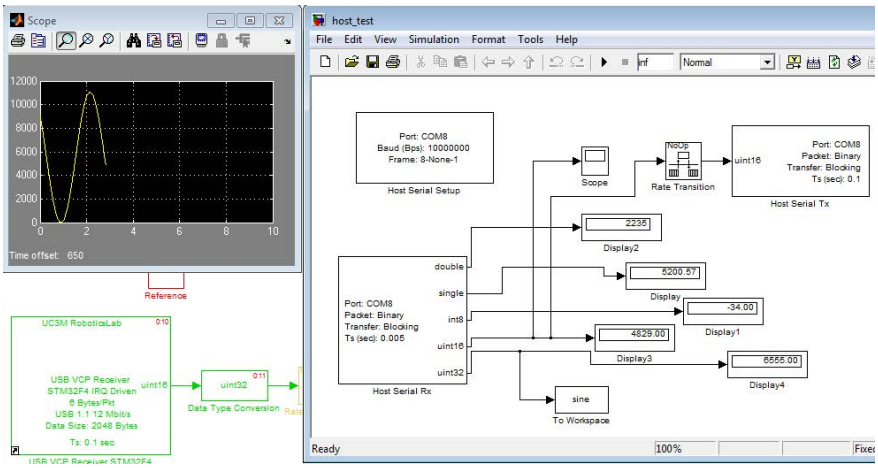

Figure 4: Simulink® graphical programming enviromment, a simple data acquisition program, reading and storing data received from a STM32F4 target via USB.

Once the needed blocksets for the RCP system are installed, the firmware is developed as a Simulink® block model, with Matlab® scripts if needed. The code generation, compiling and loading into the MCU are completely automatic and transparent to the user. Figure 5 illustrates the firmware development stages. Source code generation

and compiling are designed to use one of these three different compiler environments: the free GNU-ARM, and the commercial Keil Uvision® and IAR Ewarm®.

Figure 5: Simulink® modeling workflow using the UC3M RCP system. From left to right, Simulink generates all the required source code to for the selected compiler, and automatically loads the resulting firmware into the MCU.

Thanks to this RCP system, the development of the embedded software to control the SMA actuator and all the required testing stages have been accomplished in a very affordable and quick way.

3.2. Control Algorithm

Due to the large hysteresis area and heavily nonlinear behaviour of SMA actuators, obtaining an accurate mathematical model of the SMA actuator is a difficult task. In this paper, an innovative modelling technique is applied. This technique consists in a traditional computer aided (CAD) system identification used to compute the parameters of the control algorithm. This technique leads to a relatively quick embedded control algorithm development for different SMA actuators, with different lengths, diameters and transformation temperatures.

3.2.1. Identification of a dynamic model for the SMA actuator

The nonlinear behaviour and large hysteresis of SMA actuators make it difficult to develop control algorithms, and usually nonlinear control methods have to be applied. In the identification and modelling of the nonlinear behaviour of SMA actuators, different methodologies have been studied in the literature. In [14], the authors used a Neural Network to learn an inverse model of the hysteresis loops of a SMA actuator. Using this method to model and hysteric system is a complex task because the output depends on the current input and the previous input as well as on the previous outputs, and also the dataset has to contain information to determine whether the system state is in the ascending or in the descending part of the hysteresis loop. Selecting the appropriate training sets is critical and has to be done carefully to avoid identification problems. Another option to model the hysteric behaviour of SMAs is to use operator-based models, like the Preisach model [15][16][17], the Krasnosel'skii-Pokrovskii model [18] or the Prandtl-Ishlinskii model [19]. The common drawback of these methods is the great number of parameters they use (thresholds, weights, number of operators). These parameters have to be identified experimentally by means of optimization algorithms and are very dependent on the physical properties of the actuator, like the diameter of the SMA wire, its length or the applied bias force. There are other nonlinear system identification methods such as the Hammerstein-Wiener model [20] or the Laguerre filters [21]. In this paper, to identify the behaviour of the designed SMA actuator, the Hammerstein-Wiener method has been used because of its simplicity with respect to the other mentioned models.

When there is a nonlinear relationship between the inputs and the output of a system, sometimes this relationship can be decomposed into two or more interconnected elements. The dynamics of the system can be represented by a linear transfer function and its nonlinear behaviour can be modeled using nonlinear functions of inputs and outputs of the linear system. The Hammerstein-Wiener model achieves this configuration as a series connection of static nonlinear blocks with a dynamic linear block.

The Hammerstein-Wiener model is used to model other nonlinear systems aside from SMA actuators. It is widely used to model electro-mechanical systems and radio frequency components, in audio and speech processing and in predictive control of chemical processes. These identification models are popular because they have a convenient

block representation, transparent relationship to linear systems, and are easier to implement than heavy-duty nonlinear models (such as neural networks and Volterra models) [1]. The block structure of the Hammerstein-Wiener model can be seen in Figure 6.

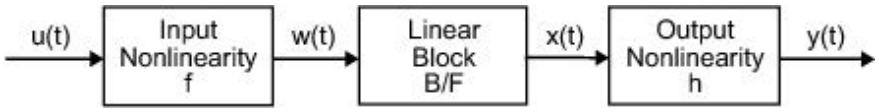

Figure 6: Structure of Hammerstein-Wiener model

where:

- $w(t) = f(u(t))$ is a nonlinear function transforming input data $u(t)$. $w(t)$ has the same dimension as $u(t)$.
- $x(t) = (B/F)w(t)$ is a linear transfer function. $x(t)$ has the same dimension as $y(t)$. B and F are similar to polynomials in the linear Output-Error model.
- $y(t) = h(x(t))$ is a nonlinear function that maps the output of the linear block to the system output.

The structure of the Hammerstein Wiener model is composed of two nonlinear models and one linear model. The first one, $w(t) = f(u(t))$, is computed from the input data. This term represents an input nonlinearity, a static function, where the value given in time t depends on the input value in time t. The second block represents a linear transfer function $x(t) = (B/F)w(t)$. In this case, the transfer function (B/F) can be configured specifying the order of the numerator B as well as the order of the denominator F. The nonlinear output block is represented using a nonlinear function $y(t) = h(x(t))$. Similar to the input nonlinear function, the output nonlinear function is a static function.

To identify the model of the SMA actuator, the input signal of the Hammerstein-Wiener model is the duty cycle of the PWM control signal, and the output signal is the real position of the actuator. One problem encountered when identifying the model is that during the elongation phase there is no control signal, to allow the SMA wire to cool. Because of this, the model can not be correctly identified during the cooling phases of the wire. This actuation phase has been modelled using MATLAB's curve fitting toolbox. With this method, Equation (2), capable of approximately simulate the behaviour of the SMA wire during the cooling phase, has been obtained. Equation (2) parameters are shown in Table 1. The input signal used in the identification process is shown in Figure 7.

$$pos(t) = a_1 * e^{-(\frac{t-b_1}{c_1})^2} + a_2 * e^{-(\frac{t-b_2}{c_2})^2} + a_3 * e^{-(\frac{t-b_3}{c_3})^2} \tag{2}$$

a_1	-7707	a_2	-901.3	a_3	$7.317 * 10^{15}$
b_1	-0.9936	b_2	1.803	b_3	-246.5
c_1	2.025	c_2	1.367	c_3	47.59

Table 1: Equation (2) parameters

[1] http://www.mathworks.es/es/help/ident/ug/identifying-hammerstein-wiener-models.html

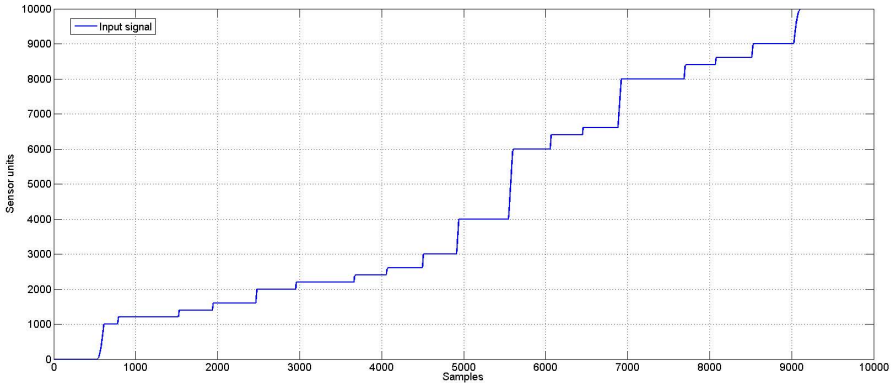

Figure 7: Input signal used in the identification process

To measure the displacement of the actuator, a digital hall effect linear encoder with a resolution of $0.488\mu m$ has been used. The signal from the position sensor is affected by electric noise. In order to use this signal in the identification process, it has been pre-processed with various filters to attenuate the noise as much as possible. To identify the model of the SMA actuator, the System Identification Toolbox of MATLAB® has been used. This tool allows to identify both the linear and nonlinear models using the Hammerstein-Wiener method, among others. The nonlinear input block of the Hammerstein-Wiener model is a wavelet network nonlinearity estimator. A piecewise-linear nonlinear estimator has been used in the output nonlinear block of the model. The linear block is characterized by a 3^{rd} order transfer function.

The result of this identification is shown in Figure 8. The approximation of the model is about 93.78%. Despite the nonlinear behaviour of the SMA actuator, the achieved model is quite precise and has a good fitting. The error of the estimated system is caused by the nonlinearity of the SMA.

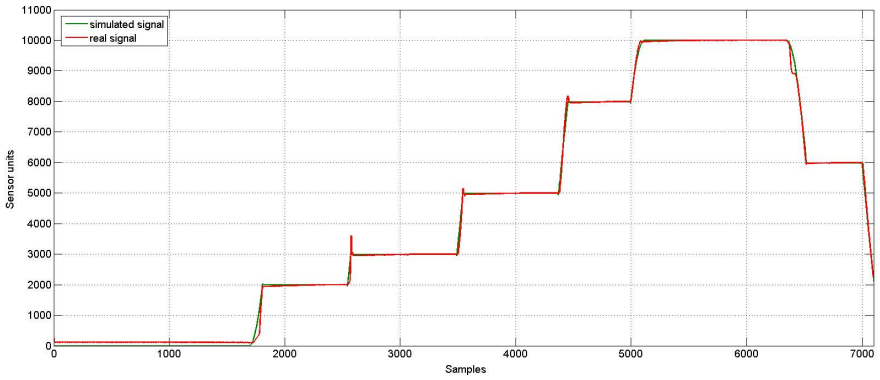

Figure 8: Result of the measured and simulated model

A position and velocity controller has been implemented and thanks to the identified system, the parameters of the control algorithm can be estimated via simulation by automatic tuning toolboxes.

3.2.2. Control Algorithm Implementation

The implemented control is based on a simultaneous velocity and position control for the SMA actuator. Both controllers are running in parallel in the embedded RCP hardware. At a given time, only one of the controllers, position or velocity is being executed, achieving a high computational efficiency, also by using single precision floating

point calculations. The control algorithm is a Proportional-Integral-Derivative (PID) for both velocity and position control. Figure 9 represents a SMA actuator driver with the general controller scheme.

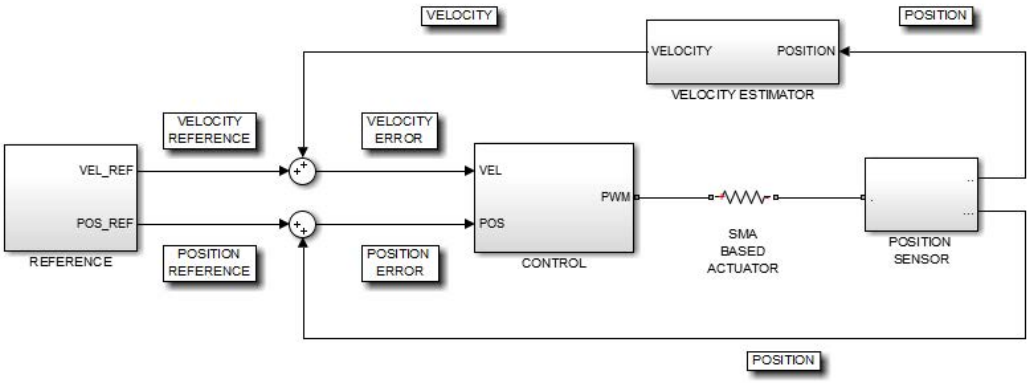

Figure 9: General implemented SMA driver scheme, including all the needed control and logic computations as well the communications interfaces

A communications interface along with its processing logic is used to receive the position and velocity references from a PC connected to the MCU. The position feedback required by the control algorithm is measured by a high resolution hall effect linear encoder, that provides the position information in a purely digital form. The position sensor uses an Inter-Integrated Circuit (I2C) bus interface that connects directly to the RCP system. The velocity feedback required by the velocity controller is estimated from the data provided by this position sensor.

The control algorithm itself resides inside the block called ”Control” in Figure 9. The block diagram of this control algorithm can be seen in Figure 10. There are two PID controllers: the bottom one corresponds to the position controller and the PID controller at the top corresponds to the velocity controller. The gain values for each controller are computed automatically using CAD assistance, thanks to the initial system identification. As already mentioned above, the system identification does not totally model the hysteresis of the SMA actuator in an effective way. These discrepancies between the modelled system and the real actuator are caused by the dependence of model to some physical parameters like the diameter of the SMA wire or the bias weight used in the identification process. Furthermore, as discussed before, the elongation phase of the actuator has been modelled by Equation (2), obtained using MATLAB’s curve fitting toolbox due to the lack of a control signal during this phase. This makes this part of the model less accurate than the one modelled with the Hammerstein-Wiener method and introduces some errors between the real and the simulated system. However, the control algorithm is able to compensate this errors and, as shown in the experimental tests section, the controller is able to follow the position reference quite accurately without overshoot. Additionally, the implemented control algorithm effectively prevents overheating the SMA wire, which has a strong impact on the service life of actuator.

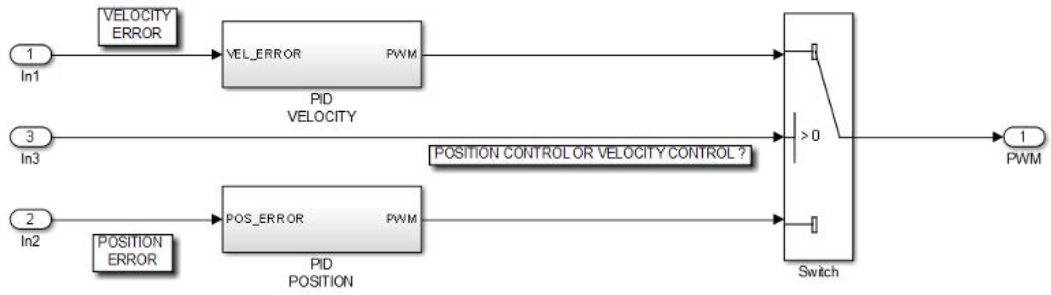

Figure 10: General implemented SMA driver scheme, it includes all needed control and logic computations as well the communications interfaces

4. Experimental tests

The results obtained in the experimental tests carried out to study the operation of the designed actuator as well as the results of the implemented position and velocity control are presented below.

4.1. Actuator contraction tests

To validate the design of the actuator, some tests have been performed in which the total displacement of the actuator has been measured. The experiments have been conducted using two different actuators, one with a length of 205mm (short actuator) and another one with a length of 395mm (long actuator). The flexible nylon sheath has an external diameter of 3.3mm and an internal diameter of 1.5mm. The actuator to be tested is fixed to a wooden surface and has a weight of 300g attached to its movable end in order to exert the bias force needed to restore the total length of the SMA wire in its martensite phase. A black marker in the nylon wire that connects the movable end of the actuator with the weight is used to visually measure how much the weight is displaced by the action of the actuator.

The SMA wire used in this tests is a SmartFlex015® wire, a NiTi wire manufactured by SAES® Getters, whose main features are [22]:

- Diameter $\text{ø} = 150 * 10^{-6} m$.
- Max. force $F_{max} = 6.2N$.
- Max. stroke $\Delta L_{max} = 5\%$.
- Austenite start temperature $A_s = 60°C$.
- Austenite finish temperature $A_f = 80°C$.
- Martensite start temperature $M_s = 55°C$.
- Martensite finish temperature $M_f = 40°C$.

First test: short actuator with three turns of wire

The first experiment has been performed using the short actuator with three loops of the SMA wire inside the Bowden cable sheath. The relevant parameters of this experiment are:

- Length of the actuator $L_{act} = 205mm$
- Number of turns of the SMA wire $n_{tur} = 3$
- Length of the SMA wire $L_{SMA} = 570mm$
- Theoretical displacement (3%) $\Delta L_{SMA_{theo}} = 17.1mm$

The measured displacement in this first test has not been as expected, with a value of about $\Delta L_{SMA_{exp}} = 8mm$. Additionally, the contraction of the SMA wire has been irregular and jerky. After deactivating the actuator, the SMA wire has not recovered its original length. Our hypothesis is that the friction of the three turns of the SMA wire inside the Bowden cable sheath between themselves causes the observed behaviour. It is also possible that inside the Bowden cable sheath, the three branches of the SMA wire are twisted with each other. This, added to the friction force, overcomes the bias force provided by the weight and the wire does not relax to its original length.

Another possible explanation to the observed behaviour is that the Bowden cable sheath is acting as an insulating barrier, impeding the SMA wire reaching the martensite transformation temperature. However, it can be demonstrated how the nylon sheath does not decrease heat flow from the SMA wire to the air. The thermal system comprising the SMA wire and the Bowden cable sheath is analysed with the lumped capacitance method as a thermal circuit. In this way, the thermal resistance (the measurement of the resistance of a material to heat flow) of each element of the system can be calculated in order to compare the capacity to transmit heat when using the wire in still air to the capacity when using it inside the sheath. Let

$h_{SMA} = 102.29 \frac{W}{m^2 K}$ (convective heat transfer coefficient of the SMA wire)

$h_{nylon} = 12.3 \frac{W}{m^2 K}$ (convective heat transfer coefficient of the nylon sheath)

$k_{nylon} = 0.25 \frac{W}{mK}$ (thermal conductivity of nylon)

$r_{int} = 0.75 * 10^{-3} m$ (internal radius of the nylon sheath)

$r_{ext} = 1.65 * 10^{-3} m$ (external radius of the nylon sheath)

$L_{sheath} = 0.205m$ (length of the nylon sheath)

$A_{SMA} = 2.69 * 10^{-4} m^2$ (surface area of the SMA wire)

$A_{sheath} = 2.13 * 10^{-3} m^2$ (surface area of the nylon sheath)

The convective thermal resistance of the SMA wire in still air is computed as:

$$R_{SMA_{conv}} = \frac{1}{h_{SMA} * A_{SMA}} = 36.34 K/W \tag{3}$$

For the case of the SMA wire inside the nylon sheath, the thermal resistance of the system is the sum of the conductive and the convective thermal resistances of the sheath:

$$R_{nylon_{cond}} = \frac{ln(r_{ext}/r_{int})}{2 * \pi * k_{nylon} * L_{sheath}} = 2.45 K/W \tag{4}$$

$$R_{nylon_{conv}} = \frac{1}{h_{nylon} * A_{sheath}} = 38.17 K/W \tag{5}$$

$$R_{tot} = R_{nylon_{cond}} + R_{nylon_{conv}} = 40.62 K/W \tag{6}$$

With the above calculations it is demonstrated that the nylon sheath does not act as a thermal insulator. Although with the nylon sheath a conductive heat transfer term is introduced, the conductive thermal resistance is small and heat flows from the inside to the outside of the sheath with little impediment. Also, even though the convective heat transfer coefficient of nylon is much smaller than that of the SMA, the larger surface area of the sheath compensates this fact and its convective thermal resistance is only slightly higher than the one of the SMA.

Second test: short actuator with two turns of wire

Taking into account the outcome of the first experiment, in the second experiment the number of loops inside the Bowden cable sheath of the short actuator has been reduced to two, so only one pulley is used. The parameters of this experiment are:

- Length of the actuator $L_{act} = 205mm$
- Number of turns of the SMA wire $n_{tur} = 2$
- Length of the SMA wire $L_{SMA} = 380mm$
- Theoretical displacement (3%) $\Delta L_{SMA_{theo}} = 11.4mm$

The measured displacement has been $\Delta L_{SMA_{exp}} = 12mm$. This value is about a 6% of the total length of the actuator, doubling the percentage of the displacement in terms of the total length of the SMA wire. This time both the contraction and the relaxation of the SMA wire have been regular and smooth.

Third test: long actuator with two turns of wire

In the third experiment, the operation of the actuator when the Bowden cable sheath is bent has been tested. For this experiment, the long actuator with two loops of the SMA wire inside the Bowden cable sheath has been used. The actuator has been bent with a Ω shape, as Figure 3 shows. The important parameters of this experiment are:

- Length of the actuator $L_{act} = 395mm$
- Number of turns of the SMA wire $n_{tur} = 2$
- Length of the SMA wire $L_{SMA} = 760mm$
- Wrap angle (Σ bending angles) $\Theta = 236° = 4.12rad$
- Theoretical displacement (3%) $\Delta L_{SMA_{theo}} = 22.8mm$

The measured displacement has been $\Delta L_{SMA_{exp}} \simeq 20mm$, about a 2.6% of the length of the SMA wire. However, the SMA wire has contracted again in an irregular and jerky way. When turning off the electric current, the wire relaxes completely, but very slowly. One reason for these problems is related to the material of the Bowden cable sheath as well as the bending angles of the actuator. In [23], frictional losses of Bowden cables are modelled as the frictional losses of a cable sliding at a constant velocity around a stationary cylinder, with a wrap angle Θ equal to the sum of all bending angles of the Bowden transmission. The force transmission efficiency is defined as:

$$F_{S1}/F_{S2} \cong e^{-\mu\Theta} \tag{7}$$

where μ is the coefficient of sliding friction and Θ the wrap angle in radians.

Applying Equation (7) to our case, with a $\mu_{nylon} = 0.35$ and a $\Theta = 4.12rad$, the force transmission efficiency is $F_{S1}/F_{S2} \simeq 0.24$. This is a low value, and can be clearly improved using a material with a lower friction coefficient for the Bowden cable sheath. For example, if a PTFE tube would be used ($\mu_{PTFE} = 0.04$), the force transmission efficiency for the same wrap angle would be $F_{S1}/F_{S2} \simeq 0.85$.

Fourth test: long actuator with individual PTFE sheaths

In the light of the results obtained in the previous tests, some modifications in the design of the actuator have been made. To avoid the limitation in the number of loops of the SMA wire due to the friction of the SMA wire branches between themselves, each branch has been routed in a separate narrow-gauge sheath. This will also avoid twisting between the branches of the SMA wire. Furthermore, to reduce friction between the SMA wire and the Bowden cable sheaths and thus increase the force transmission efficiency of the actuator, the nylon sheaths have been replaced by flexible PTFE tubes.

This experiment has been performed with the long actuator with three loops of the SMA wire inside individual narrow-gauge Bowden cable sheaths, now that the number of loops is not a limiting factor. As in the previous test, the actuator has been bent with a Ω shape. The parameters of this experiment are:

- Length of the actuator $L_{act} = 395mm$
- Number of turns of the SMA wire $n_{tur} = 3$
- Length of the SMA wire $L_{SMA} = 1185mm$
- Wrap angle (Σ bending angles) $\Theta = 236° = 4.12rad$
- Theoretical displacement (3%) $\Delta L_{SMA_{theo}} = 35.6mm$

The measured displacement has been $\Delta L_{SMA_{exp}} = 36.2mm$. This means that the displacement produced by the actuator is about a 9% of its total length, which is three times the percentage of the displacement in terms of the total length of the SMA wire. As expected, the actuation in both the contraction phase and the elongation phase has been regular and without abrupt changes and the wire is able to recover its entire length in the cooling phase.

4.2. Control tests

To test the effectiveness of the developed control algorithm, a very simple test bench, shown in Figure 11, has been built using 3D printed parts. The test bench has a magnetic linear position sensor to measure the contraction of the wire and obtain the position feedback for the control algorithm. It also houses a bias spring to provide the necessary force to recover the initial length of the SMA wire during the cooling phase. One of the ends of the SMA actuator is fixed to the table while the other end is attached to a structure containing a movable piece, the bias spring and the position sensor. The movable end of the actuator is crimped to the movable part of the structure, which has a magnetic strip on one side. When the actuator contracts, the movable part is displaced and the position sensor measures the displacement of the magnetic strip. The resolution of the magnetic sensor is $0.488\mu m$. The control tests have been performed with the short actuator.

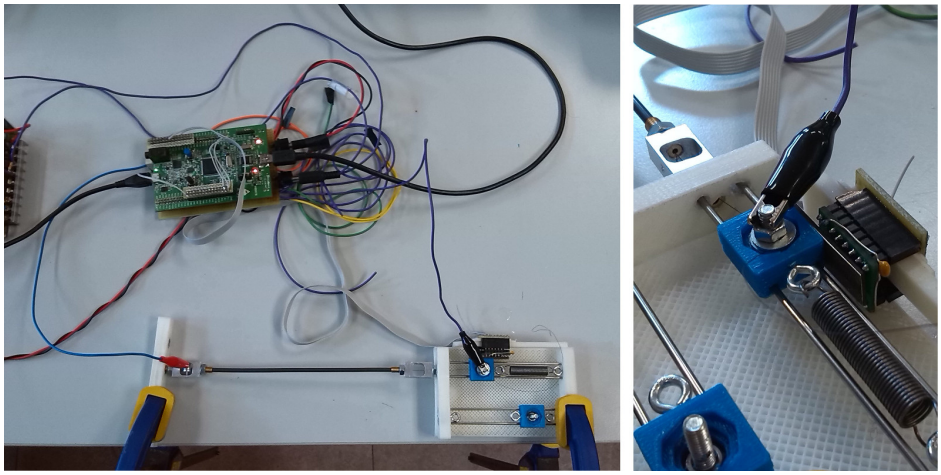

Figure 11: Setup for the control experiments (left) and detail of the position sensor and bias spring (right)

Firstly, the control algorithm has been tested tuning the gains experimentally. The result of this first experiment is shown in Figure 12. The controller makes the actuator follow a $0.25Hz$ sinusoidal reference. As can be seen, the response of the controller oscillates around the reference, especially in the latter half of the contraction phase when the force exerted by the bias spring is greater.

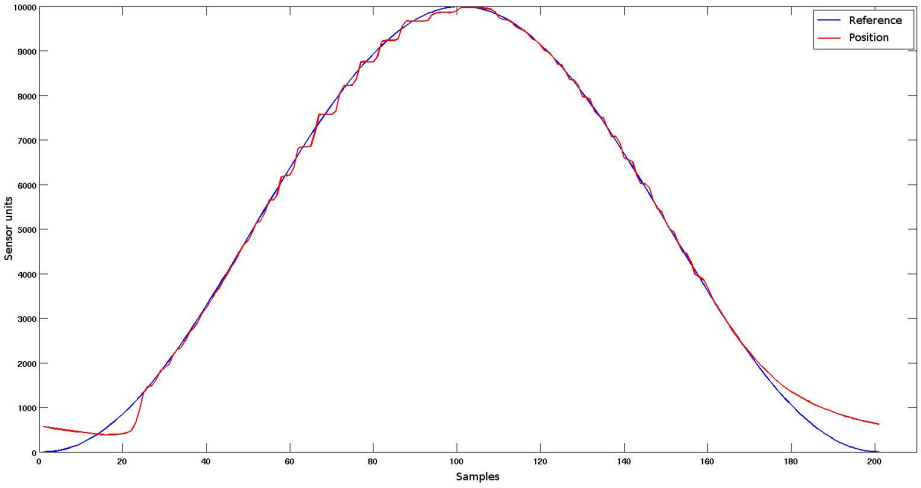

Figure 12: PID control with gains adjusted experimentally following a $0.25Hz$ sine reference

The response of the previous experiment has been improved computing the gains of the PID controller using the Hammerstein-Wiener model of the SMA actuator. The result of the second experiment can be seen in Figure 13. The control of the actuator is smoother than in the previous test, but due to its nonlinearities, there is some oscillation at the beginning of the relaxation phase. From the second half of the relaxation phase, the actuator is not able to follow the reference, due to the cooling time of SMA wire.

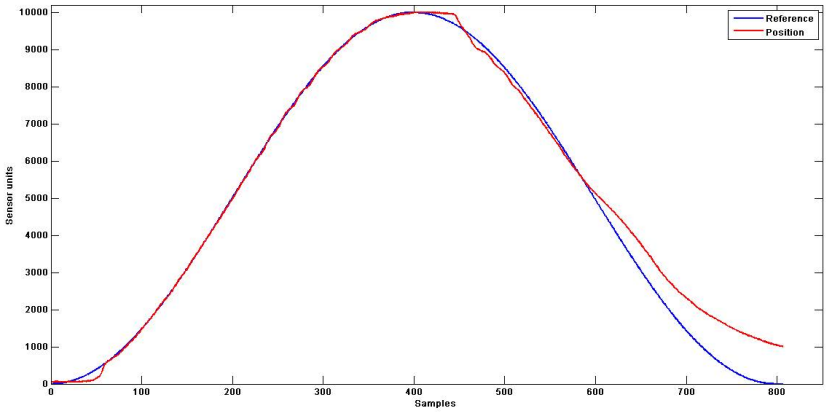

Figure 13: PID control with gains adjusted by the Hammerstein-Wiener model following a $0.25Hz$ sine reference

The following experiments are intended to demonstrate the operation of velocity control. Figure 14 shows the performance of the controller when the actuator follows a reference of 10000 sensor units ($4880\mu m$) at a velocity of $1290\mu m/s$. The actuator follows the reference quite accurately, maintaining a constant position without oscillations. Again, during the relaxation phase the actuator is not able to follow the reference because of the cooling time of the

SMA wire.

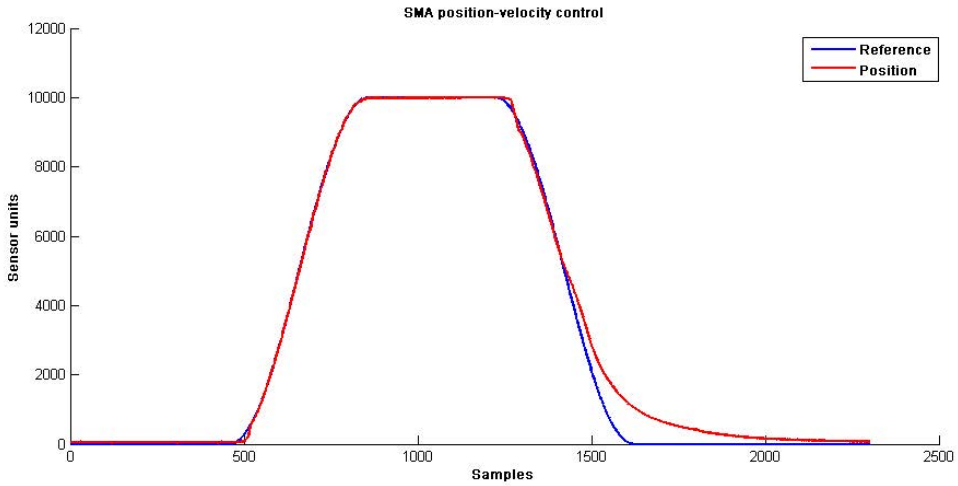

Figure 14: Position-velocity control for a position of 10000 sensor units ($4880\mu m$) and a velocity of $1290\mu m/s$

As shown in Figure 15, the controller is able to make the actuator follow the same reference as in the previous experiment but at a higher velocity of $2870\mu m/s$. However, the difference between the reference and the real position of the actuator in the relaxation phase is more pronounced due to the increased velocity and the same cooling time.

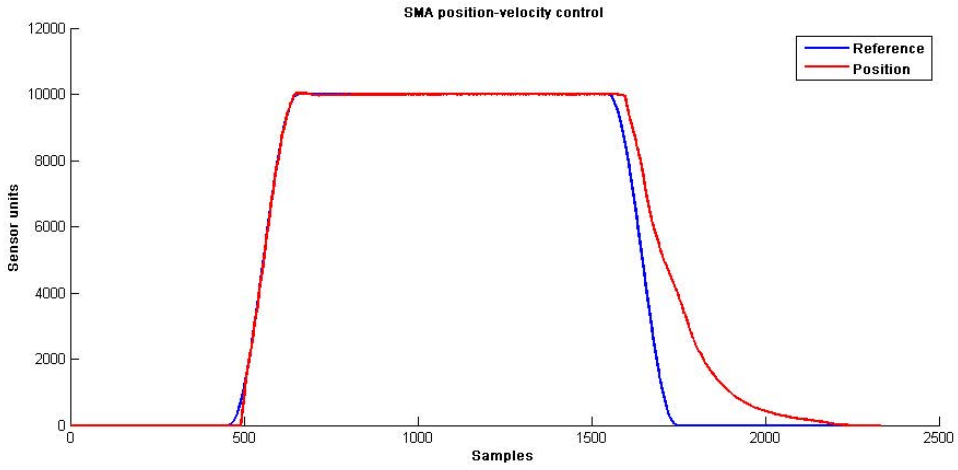

Figure 15: Position-velocity control for a position of 10000 sensor units ($4880\mu m$) and a velocity of $2870\mu m/s$

Finally, Figure 16 shows a periodic series of contractions and relaxations of the actuator following a sinusoidal reference of $0.125Hz$.

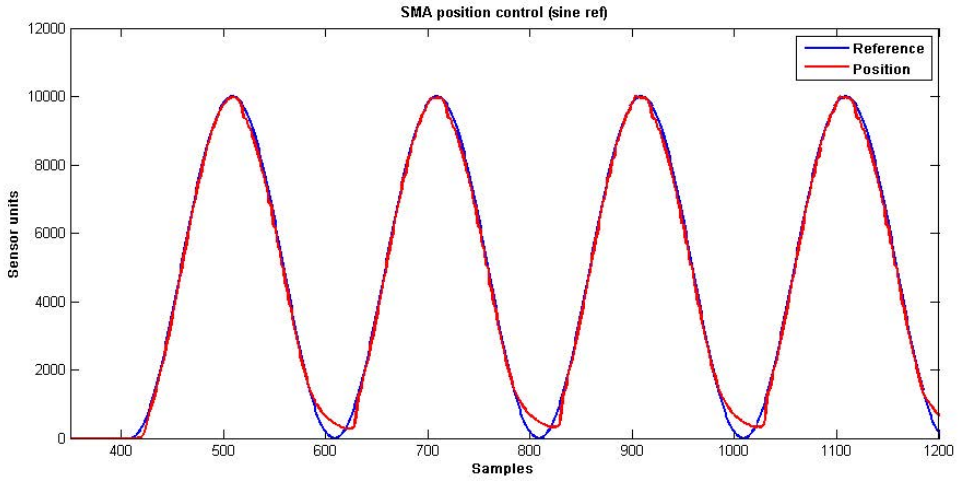

Figure 16: Position-velocity control for a $0.125Hz$ sinusoidal reference

5. Application of the high-displacement flexible SMA actuator in a wrist exoskeleton

As stated before, the main purpose of the designed flexible SMA actuator is its application in soft wearable robots. Because of the limited time response of SMAs, its use actuating soft exoskeletons is restricted to those devices that do not require high actuation rates. Usually, physical therapy rehabilitation exoskeletons, oriented to train and eventually restore the motor function of the affected limb, match this requirement as the rehabilitation exercises are slow to do no harm to the patient. With respect to the tensile force needed to mobilize an affected limb, force requirements can be easily met using a wire with a larger diameter capable of exerting a greater force, or several thin wires in parallel.

To demonstrate the feasibility of using the presented actuator in a rehabilitation-oriented soft wearable robot, a wrist mobilization prototype device driven by the flexible SMA actuator has been designed. This wrist exoskeleton is intended to actively actuate the extension movement of the wrist, while the flexion movement to a neutral position is passive. Being a soft exoskeleton, the structure of the device does not consist of rigid links joining the forearm with the hand and there is no rotational joint parallel to the sagittal plane of the wrist; it only has a few rigid parts, intended to fix the actuator ends. This greatly reduces singularities in the workspace of the device, improves kinematic compatibility since there is no joint misalignment and the device is more adaptable to different users' body sizes, more comfortable and more portable than standard rigid solutions.

The designed device allows a wrist extension of up to 45° when the actuator contracts. To produce this angular displacement, the actuator has to exert a linear displacement of about $36mm$, which implies a SMA wire with a length of $1.2m$ (if the wire is contracted a 3% of its length to increment its service life). Upon cooling, the recovery force that elongates the SMA wire to its initial length is exerted by the weight of the hand. Thanks to the relatively slow cooling time of the SMA actuator, the wrist is flexed to the neutral position at a regular rate and in a non abrupt way. To exert the necessary force to extend the wrist, a SMA wire with a diameter of $0.5mm$ capable of producing a force of $35N$ has been used.

Thanks to the flexible design of the actuator presented in this paper, this $1.2m$ long SMA wire can be located on the user's arm, adapting to its shape and to its movements without being uncomfortable, as shown in Figure 17. One of the ends of the flexible sheath of the actuator is fixed to a foam armband, whose diameter can be adjusted by means of Velcro straps, located around the arm near the user's shoulder. The other end of the sheath is fixed to another foam armband located at the end of the user's forearm. In order to mobilize the hand and thus extend the wrist, the movable end of the actuator is crimped to a simple rigid piece which is placed over the wearer's hand. When the SMA wire is contracted, this piece is pulled and the extension of the wrist is achieved. To make this system more comfortable, the

user wears a neoprene glove above which this piece is placed. To measure the bending angle of the wrist in order to have a position feedback for the control loop, a flexible potentiometer is placed over the wrist. This sensor increases its electrical resistance when its bending angle is increased. This variation is converted to a voltage variation with a very simple circuit and used as the measurement of the bending angle of the wrist.

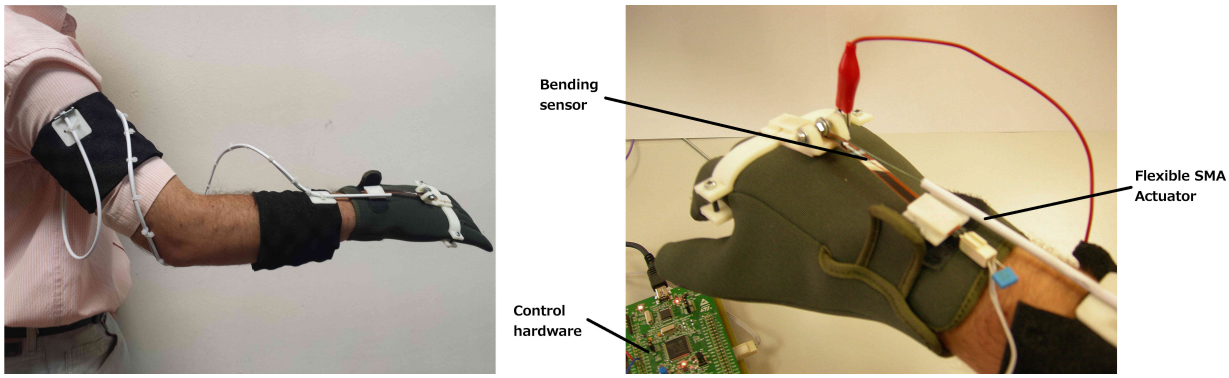

Figure 17: Wrist exoskeleton prototype: arrangement of the flexible actuator around the arm (left); detailed view of the device (right)

It should be noted that the described wrist exoskeleton is a proof of concept device intended to show that the flexible SMA actuator presented in this paper can be used to mobilize a human limb in a soft wearable robot, and for this reason, it has not been designed as a real rehabilitation device following design guidelines and constraints related with this field of application, and has been tested in healthy subjects and not in impaired people.

6. Conclusions

A high-strain flexible SMA actuator has been presented. Based on the principle of Bowden cable actuation, that makes it possible to bend the device, the designed actuator has a great potential to be used in soft wearable robots. The proposed design achieves a great linear displacement compared to the total length of the actuator. The tests carried out to assess the performance of the actuator have helped refine its design.

After finding out how the number of turns of the SMA wire inside the Bowden cable sheath affects the performance, because of the friction of the SMA wire branches between each other, we conclude that it is a better solution to route each of the turns of the SMA wire through individual narrow-gauge tubes. Having each branch of the looped SMA wire routed into individual sheaths should allow to design an actuator with as many loops as desired, thus increasing the total displacement that the actuator can produce. In this case, the number of pulleys that the actuator should require would be the limiting factor in terms of friction losses and total weight of the actuator.

The effect of the material of the Bowden cable sheath has also been tested. The sliding friction coefficient of the material greatly affects the force transmission efficiency. Using materials with a lower friction coefficient, like PTFE, further improves the performance of the actuator.

Regarding the control algorithm implementation, the used RCP system has allowed to develop the algorithm in a simple and quick way. Also, the use of the Hammerstein-Wiener model to identify the model of the SMA actuator has allowed to calculate the PID gains in a more optimal and fast way than experimentally. The implemented control algorithm is able to make the actuator follow a reference at different velocities and with an acceptable accuracy. Due to the hysteresis of the actuator, the controller does not work perfectly. This issue can be addressed by introducing an inverse hysteresis model as a feedforward term for the controller.

Finally, a very simple wrist exoskeleton driven by the designed actuator has been built. This device uses a minimum number of rigid parts, following the design philosophy of soft wearable robotics. This device, that extends the wearer's wrist up to 45°, has served to demonstrate that the concept of flexible actuator presented in this paper can be applied to those wearable robots that do not require high rates of actuation, such as physical therapy rehabilitation exoskeletons.

7. Acknowledgements

The research was funded by the HYPER Project (Consolider-Ingenio 2010) and the STAMAS Project (EU Seventh Framework Programme). The research leading to these results also has received funding from the RoboCity2030-II-CM project (S2009/DPI-1559), funded by "Programas de Actividades I + D en la Comunidad de Madrid" and co-funded by Structural Funds of the European Union.

8. Appendix: convective heat transfer coefficients calculation

Assuming the SMA wire as a horizontal cylinder, its convective heat transfer coefficient is computed as follows. Let

$T_{air} = 20°C$ (air temperature)

$\rho_{air} = 1.205 \frac{Kg}{m^3}$ (air density)

$\mu_{air} = 15.11 * 10^{-6} \frac{m^2}{s}$ (air viscosity)

$C_{P_{air}} = 1005 \frac{J}{Kg°K}$ (air specific heat capacity)

$k_{air} = 0.0257 \frac{J}{smK}$ (air thermal conductivity)

$\beta_{air} = 3.047 * 10^{-3} ° K^{-1}$ (air thermal expansion coefficient)

$T_{SMA} = 90°C$ (SMA wire surface temperature in austenite phase)

$\emptyset_{SMA} = 150 * 10^{-6} m$ (SMA wire diameter)

$T_{sheath} = 40°C$ (nylon sheath surface temperature)

$\emptyset_{sheath} = 3.3 * 10^{-3} m$ (nylon sheath outer diameter)

First, the Grashof number (8) and the Prandtl number (9) are computed as:

$$Gr_{SMA} = \frac{\emptyset_{SMA}^3 * \rho_{air}^2 * g * (T_{SMA} - T_{air}) * \beta_{air}}{\mu_{air}^2} = 0.045 \tag{8}$$

$$Pr_{SMA} = \frac{\mu_{air} * C_{P_{air}}}{k_{air}} = 0.59 \tag{9}$$

With the results from equations 8 and 9, the Rayleigh number is computed:

$$Ra_{SMA} = Gr_{SMA} * Pr_{SMA} = 0.0265 \tag{10}$$

From this result, the Nusselt number, and hence the convective heat transfer coefficient of the SMA wire, are computed:

$$Nu_{SMA} = (0.60 + \frac{0.387 * Ra_{SMA}^{1/6}}{(1 + (0.559/Pr_{SMA})^{9/16})^{8/27}})^2 = 0.597 \tag{11}$$

$$Nu_{SMA} = \frac{h_{SMA} * \emptyset_{SMA}}{k_{air}} \Rightarrow h_{SMA} = \frac{Nu_{SMA} * k_{air}}{\emptyset_{SMA}} = 102.29 \frac{W}{m^2 K} \tag{12}$$

Similarly, the convective heat transfer coefficient of the nylon sheath can be calculated as:

$$Gr_{sheath} = \frac{\emptyset^3_{sheath} * \rho^2_{air} * g * (T_{sheath} - T_{air}) * \beta_{air}}{\mu^2_{air}} = 136,63 \tag{13}$$

$$Pr_{sheath} = \frac{\mu_{air} * C_{P_{air}}}{k_{air}} = 0.59 \tag{14}$$

$$Ra_{sheath} = Gr_{sheath} * Pr_{sheath} = 80.61 \tag{15}$$

$$Nu_{sheath} = (0.60 + \frac{0.387 * Ra^{1/6}_{sheath}}{(1 + (0.559/Pr_{sheath})^{9/16})^{8/27}})^2 = 1.58 \tag{16}$$

$$Nu_{sheath} = \frac{h_{sheath} * \emptyset_{sheath}}{k_{air}} \Rightarrow h_{sheath} = \frac{Nu_{sheath} * k_{air}}{\emptyset_{sheath}} = 12.3 \frac{W}{m^2 K} \tag{17}$$

References

[1] J. L. Pons and E. Rocon, Scaling of piezoelectric actuators: a comparison with traditional and other new technologies, Boletín de la Sociedad Española de Cerámica y Vidrio 45 (2006) 132-138.

[2] Technical characteristics of Flexinol® actuator wires, Tech. Sheet, Dynalloy Inc.

[3] K. Andrianesis and A. Tzes, Design of an Innovative Prosthetic Hand with Compact Shape Memory Alloy Actuators, Control & Automation (MED), 2013 21st Mediterranean Conference on (2013) 697-702.

[4] S. Pittaccio and S. Viscuso, Shape Memory Actuators for Medical Rehabilitation and Neuroscience, in: G. Berselli, R. Vertechy and G. Vassura (Eds.), Smart Actuation and Sensing Systems - Recent Advances and Future Challenges, 2012, pp. 83-120.

[5] G. Song, B. Kelly and B.N. Agrawal, Active position control of a shape memory alloy wire actuated composite beam, Smart Materials and Structures 9 (2000).

[6] J. Jang, C. K. Ahn, S. Han, and W. H. Kwon, Rapid Control Prototyping for Robot Soccer System using SIMTool, Proc. SICE-ICASE International Joint Conference 2 (2006) 30353039.

[7] X. Chen, X. Gong, H. Zhou, Z. Xu, Y. Xu, and C. Kang, An economical rapid control prototyping system design with Matlab/Simulink and TMS320F2812 DSP, IMECS (2010).

[8] G. Chindris and M. Muresan, Deploying Simulink models into system on-chip structures, ISSE, (2006), 313-317.

[9] D. Hcrcog, A. Kapun, and K. Jezernik, Implementation and usage of a freely available real-time operating system on an embedded robot controller, Elektroteh Vestn (Slovenia)75 (2008) 75136142.

[10] A. Flores, D. Copaci, A. Martín, D. Blanco, and L. Moreno, Smooth and accurate control of multiple shape memory alloys based actuators via low cost embedded hardware, IROS (2012).

[11] EE Times Group, 2011 embedded market study, Tech. Report (2011).

[12] EE Times Group, 2013 embedded market study, Tech. Report (2013).

[13] O. Pinzon-Ardila, L. Angel, and M. Useche, xPC target an option for position control of robotic manipulators, LARC (2011) 16.

[14] E. Asua, V. Etxebarria, A. Garcia-Arribas, Micropositioning control using shape memory alloys, In: Proceedings of IEEE conference on control applications CCA2006 (2006) 3229-34.

[15] X. Tan, R. V. Iyer, Modelling and control of hysteresis, IEEE Control Systems Magazine 29(1) (2009) 26-28.

[16] K. K. Ahn, N. B. Kha, Improvement of the performance of hysteresis compensation in SMA actuators by using inverse Preisach model in closed-loop control system, Journal of Mechanical Science and Technology 20(5) (2006) 634-642.

[17] K. K. Ahn, N. B. Kha, Internal model control for shape memory alloy actuators using fuzzy based Preisach model, Sensors and Actuators, A: Physical 136(2) (2007) 730-741.

[18] M. R. Zakerzadeh, H. Sayyaadi, M. A. Vaziri Zanjani, Characterizing Hysteresis Nonlinearity Behavior of SMA Actuators by Krasnosel'skii-Pokrovskii Model, Applied Mathematics 1(1) (2011) 28-38.

[19] M. Al Janaideh, S. Rakheja, C-Y. Su, A generalized Prandtl-Ishlinskii model for characterizing hysteresis nonlinearities of smart actuators, Smart Mater Struct 18(4) (2009) 1-9.

[20] A. Fathi, A. Mozaffari, Identification of a dynamic model for shape memory alloy actuator using Hammerstein-Wiener gray box and mutable smart bee algorithm, International Journal of Intelligent Computing and Cybernetics 6 (2013) 328 - 357.

[21] S. Kannan, C. Giraud-Audine, E. Patoor, Identification of dynamics and hysteresis of Shape Memory Alloy (SMA) actuator using Laguerre filters, IEEE International Symposium (2008).

[22] SmartFlex® wires, Tech. Sheet, SAES® Getters.

[23] A. Schiele, P. Letier, R. van der Linde and F. van der Helm, Bowden Cable Actuator for Force-Feedback Exoskeletons, Intelligent Robots and Systems, 2006 IEEE/RSJ International Conference on (2006) 3599-3604.